Linear and Unconditionally Energy Stable Schemes for the Multi-Component Two-Phase Diffuse Interface Model with Peng-Robinson Equation of State

Chenfei Zhang[1], Hongwei Li[2], Xiaoping Zhang[3] and Lili Ju[1,*]

[1] *Department of Mathematics, University of South Carolina, Columbia, SC 29208, USA.*
[2] *School of Mathematics and Statistics, Shandong Normal University, Jinan, Shandong 250358, P.R. China.*
[3] *School of Mathematics and Statistics, Wuhan University, Wuhan, Hubei 430072, P.R. China.*

Abstract. In this paper we consider numerical solutions of the diffuse interface model with Peng-Robinson equation of state for the multi-component two-phase fluid system, which describes real states of hydrocarbon fluids in petroleum industry. A major challenge is to develop appropriate temporal discretizations to overcome the strong nonlinearity of the source term and preserve the energy dissipation law in the discrete sense. Efficient first and second order time stepping schemes are designed based on the "Invariant Energy Quadratization" approach and the stabilized method. The resulting temporal semi-discretizations by both schemes lead to linear systems that are symmetric and positive definite at each time step, and their unconditional energy stabilities are rigorously proven. Numerical experiments are presented to demonstrate accuracy and stability of the proposed schemes.

AMS subject classifications: 65M12, 65M06, 65M15

Key words: Diffuse interface model, Peng-Robinson equation of state, linear scheme, Invariant Energy Quadratization, energy stability.

1 Introduction

Many problems in the fields of science and engineering, particularly in materials science and fluid dynamics, involve flows with multiple constitutive components [11, 22, 28, 29]. A typical well-known application is the subsurface gas and oil reservoir, which contains

*Corresponding author. *Email addresses:* chenfei@math.sc.edu (C. Zhang), hwli@sdnu.edu.cn (H. Li), xpzhang.math@whu.edu.cn (X. Zhang), ju@math.sc.edu (L. Ju)

gas phase, oil phase and water phase, together with the solid phase [9]. From mathematical modeling and numerical algorithmic points of view, it is a challenge to perform numerical simulations of multiphase flows and study interfaces between phases, due to inherent nonlinearities, topological changes, and complexities of dealing with unknown moving interfaces.

There are many approaches to categorize the moving interfaces. The first method to simulate multiphase and multi-component flows is interface tracking (sharp interface modeling [24], front-tracking [10], immersed boundary [27]), and the interface is described as a zero-thickness two-dimensional entity. This approach can successfully predict the shape and dynamics of the interface, assuming that the interface tension is given. However, it can not provide information within the interface itself. The second method is the phase field model (interface capturing, diffuse interface theory) to simulate multiphase and multi-component flows [1,2,4,5,21,23], which is an increasingly popular choice for modeling the motion of multiphase and multi-component fluids. In the phase field model, a conserved order parameter such as a mass concentration that varies continuously over thin interfacial layers is introduced, and the order parameter is mostly uniform in the bulk phases. Based on this idea, sharp fluid interfaces are replaced by thin but nonzero thickness transition regions where the interfacial forces are smoothly distributed. The free interface can be automatically tracked without imposing any mathematical conditions on the moving interface. One advantage of the phase field model is that the governing system of equations in the model can be derived from the variational principle. Moreover, the phase field model usually leads to well-posed nonlinear systems that satisfy the energy dissipation law. Therefore, this model has become a well-known simulation tool to resolve the motion of free interfaces in multiple components, and has also been successfully applied to many problems in the fields of science and industry (see [12,13,30,31] and the references cited therein).

In order to study the interface between phases, the development of energy stable schemes for phase field model is an important issue. There are several popular numerical approaches to construct energy stable schemes. The first approach is the convex splitting method, which is introduced by Elliott and Stuart [3,6] and popularized by Eyre [7]. The main idea is assuming the free energy density can be split as the difference of two convex functions, where the convex part is treated implicitly and the concave part is treated explicitly. Although the convex splitting method is unconditionally energy stable and uniquely solvable, it reduces to a nonlinear system at each time step and the implementation is complicated and the computational cost is high. The second widely used approach is the stabilized method which treats the nonlinear terms explicitly, and adds an artificial stabilization term to overcome strict temporal step constraint [39,40]. This method is also energy stable and produces a linear system at each time step which is easy to implement. However, it is not easy to find the stabilization term for all problems, and it can not be unconditionally energy stable for second order scheme.

In this paper, we focus on the diffuse interface modeling of multi-component and multiphase fluid systems, and consider the energy stable schemes for a more realistic

model with Peng-Robinson equation of state (EOS). The Peng-Robinson EOS as a diffuse interface model to describe the real states of hydrocarbon fluids in the petroleum industry has become one of the most useful and successfully applied models for thermodynamic and volumetric calculations in both industrial and academic fields [20]. It has been considered as one of the best two constants third degree equations of state applicable to vapor-liquid equilibria, and volumetric and thermodynamic properties calculations for pure substances and mixtures. The structure of its energy functional is highly nonlinear and more complicated than many conventional phase field models. Therefore, the development of accurate, efficient, easy-to-implement, and energy stable numerical schemes is a very important and challenging issue. Many efforts have been devoted to designing numerical schemes with energy stability. In the work by Qiao and Sun [23], an efficient scheme for single-component systems of Peng-Robinson EOS is developed. The authors established a clean convex splitting of the total Helmholtz free energy and treated the convex and concave parts separately. However, it is not straightforward to extend the convex splitting method from single-component to multi-component systems. Fan and his collaborators designed a componentwise convex splitting scheme for diffuse interface models with Peng-Robinson EOS in [8]. Kou and Sun proposed a modified Newton's method to solve the nonlinear model and proved the maximum principle of the molar density with multi-component in [14]. Some recent developments in numerical algorithms for the multi-component diffuse interface model with Peng-Robinson EOS can be referenced to [13, 15–18].

In this work, we are devoted to designing efficient linear unconditionally energy stable numerical schemes to solve the multi-component diffuse interface model with Peng-Robinson EOS. Combining the stabilized method, the "Invariant Energy Quadratization" (IEQ) approach, which is a novel method and applicable to a large class of free energies, is adopted to develop the numerical schemes for Peng-Robinson EOS. Yang and his collaborators designed the IEQ approach by generalizing the Lagrange multiplier approach, and many phase field models have been solved by this approach [32–38]. The main idea of the IEQ method is to transform the free energy into a quadratic form of a set of auxiliary variables. Then, a new but equivalent system is obtained, which still retains the energy dissipation law in terms of the auxiliary variables. This approach enjoys the following advantages: (i) all nonlinear terms in the new system can then be discretized by semi-explicit schemes in time to produce a linear system at each time step, thus it is very efficient; (ii) the energy dissipation laws in the discrete sense are also preserved; (iii) it can be easily extended to higher-order schemes. Based on the IEQ approach, we have successfully designed the first and second order linear schemes for single-component diffuse interface model with Peng-Robinson EOS, and rigorously proved the unconditional energy stabilities [19]. Recently, Shen and his collaborators developed the scalar auxiliary variable (SAV) approach which is built upon the IEQ method. It enjoys all advantages of the IEQ approach but overcomes most of its shortcomings [25, 26]. In a future work, we shall design the unconditionally energy stable schemes for the Peng-Robinson EOS by applying the SAV approach.

The rest of this paper is organized as follows. In Section 2, the model of multi-component Peng-Robinson EOS is presented, and a linear transformation is introduced to decouple the system. In Section 3 we develop numerical schemes with respective first and second orders for time discretization of the problem, and then prove well-posedness of the resulting linear systems as well as the unconditional energy stabilities. Various 2D and 3D numerical simulations are presented to validate the proposed numerical schemes in Section 4. Finally some concluding remarks are given in Section 5.

2   Mathematical model of fluid systems with multi-component diffuse interface

A fluid system consisting of a fixed number of species on a fixed domain with a spatially uniform-distributed given temperature is considered. The total Helmholtz free energy achieves a global minimum at the equilibrium state, according to the second law of thermodynamics. We are interested in the equilibrium state of the system in this work.

We denote by M the number of components in the fluid mixture and n_i the molar concentration of the component i. Let $\mathbf{n} = (n_1, n_2, \cdots, n_M)^T$ be the molar concentrations of all components and $n = n_1 + n_2 + \cdots + n_M$ be the molar density of the fluid. According to the gradient theory, one of the most popular thermodynamic theories for inhomogeneous fluid, the total Helmholtz energy density has two contributions, one from the thermodynamic theory of homogeneous fluids and the other one from inhomogeneity of the fluid. That is

$$F(\mathbf{n}) = \int_\Omega f(\mathbf{n};T)d\mathbf{x} = F_0(\mathbf{n};T,\Omega) + F_\nabla(\mathbf{n};T,\Omega) = \int_\Omega f_0(\mathbf{n};T)d\mathbf{x} + \int_\Omega f_\nabla(\mathbf{n};T)d\mathbf{x}, \quad (2.1)$$

where T is the temperature, $F_0(\mathbf{n};T,\Omega)$ is the contribution of Helmholtz free energy density from the homogeneous fluid theory, and the $F_\nabla(\mathbf{n};T,\Omega)$ is the contribution of Helmholtz free energy density from the concentration gradient. The inhomogeneous term or the gradient contribution $f_\nabla(\mathbf{n};T)$ can be modeled by a simple quadratic relation

$$f_\nabla(\mathbf{n};T) = \frac{1}{2} \sum_{i,j=1}^M c_{ij} \nabla n_i \cdot \nabla n_j,$$

where c_{ij} is the influence parameter. The parameter c_{ij} is a function of molar concentrations and temperature. The influence parameter depends on molar concentrations only weakly, thus it is often justified to assume that c_{ij} is a constant for a given fixed temperature T.

Since the molar concentration $\mathbf{n}$ at equilibrium minimizes the total Helmholtz free energy F for a closed and conserved fluid system with temperature T, the mathematical statement of the problem is formulated as follows: find $\mathbf{n}^* \in H$ satisfying

$$F(\mathbf{n}^*) = \min_{\mathbf{n} \in H} F(\mathbf{n}), \quad (2.2)$$

subject to the constraint

$$\int_{\Omega} \mathbf{n} d\mathbf{x} = \mathbf{N}, \tag{2.3}$$

where H be a space of functions with certain regularity, $\mathbf{N} = (N_1, N_2, \cdots, N_M)^T$ is a given constant vector representing the fixed amount of material mass for each component in the system.

2.1 Peng-Robinson equation of state

The Peng-Robinson equation of state is the most popular model for computing the fluid equilibrium property of petroleum fluids in reservoir engineering and oil industries, since its publication in 1976. We briefly review the Peng-Robinson EOS in this part. The Helmholtz free energy $f_0(\mathbf{n}; T)$ of a homogeneous fluid in this model is given by

$$f_0(\mathbf{n}; T) = f_{01}(\mathbf{n}) + f_{02}(\mathbf{n}) \tag{2.4}$$

with

$$f_{01}(\mathbf{n}) = RT \sum_{i=1}^{M} n_i (\ln n_i - 1) - nRT \ln(1 - bn), \tag{2.5}$$

$$f_{02}(\mathbf{n}) = \frac{a(T)n}{2\sqrt{2}b} \ln \left(\frac{1 + (1 - \sqrt{2})bn}{1 + (1 + \sqrt{2})bn} \right), \tag{2.6}$$

where T is the temperature of the mixture and R is the universal gas constant and $n = \sum_{i=1}^{M} n_i$. The two parameters, energy parameter $a = a(T)$ which depends on temperature T, and the co-volume parameter b, are utilized in the Peng-Robinson EOS. We refer to the "Appendix" for details of these parameters.

2.2 Transformed system

Consider a fluid mixture composed of M $(M \geq 2)$ components. In order to decouple the relations between different components, a linear transformation is introduced, and as a result, the models are simplified.

The crossed influence parameters c_{ij} are generally described as the modified geometric mean of the pure component influence parameters c_i and c_j by

$$c_{ij} = (1 - \beta_{ij}) \sqrt{c_i c_j}, \tag{2.7}$$

where the parameters β_{ij} are binary interaction coefficients for the influence parameters. The influence parameter matrix is denoted by $\mathbf{C} = (c_{ij})_{i,j=1}^{M}$. In this work, suitable parameters β_{ij} are chosen such that $\mathbf{C}$ is symmetric positive definite. Thus there exists $\mathbf{Q}^T \mathbf{Q} = \mathbf{Q}\mathbf{Q}^T = I$ such that $\mathbf{C} = \mathbf{Q}\Lambda\mathbf{Q}^T$, where $\Lambda = \text{diag}(\lambda_1, \cdots, \lambda_M)$ and λ_i $(i = 1, 2, \cdots, M)$

denote the real positive eigenvalues of **C**. We can define a transformation matrix $\mathbf{Q} = [\mathbf{q}_1, \cdots, \mathbf{q}_M]$ where $\mathbf{q}_i$ $(i=1,2,\cdots,M)$ are orthonormal eigenvectors corresponding to eigenvalues λ_i $(i=1,2,\cdots,M)$. Applying this orthonormal transformation, we define a vector $\mathbf{\Phi} = [\phi_1, \cdots, \phi_M]^T$ as

$$\mathbf{\Phi} = \mathbf{Q}^T \mathbf{n}, \quad \mathbf{n} = \mathbf{Q}\mathbf{\Phi}. \tag{2.8}$$

Denote $g(\mathbf{\Phi}) = f_0(\mathbf{n}) = f_0(\mathbf{Q}\mathbf{\Phi})$. Using the relations given by (2.8), we have

$$\sum_{i,j=1}^{M} c_{ij} \nabla n_i \cdot \nabla n_j = \sum_{i=1}^{M} \lambda_i |\nabla \phi_i|^2. \tag{2.9}$$

The free energy then can be represented as

$$E(\phi) = \int_{\Omega} \left(\frac{1}{2} \sum_{i=1}^{M} \lambda_i |\nabla \phi_i|^2 + g(\phi) \right) d\mathbf{x}. \tag{2.10}$$

Based on the variational approach, we have

$$\frac{\partial \phi_i}{\partial t} = -\frac{\delta E(\phi)}{\delta \phi_i} = \lambda_i \Delta \phi_i - \frac{\partial g(\phi)}{\partial \phi_i}, \quad i=1,2,\cdots,M, \tag{2.11}$$

which is equivalent to

$$\frac{\partial \phi_i}{\partial t} = (\lambda_i \Delta \phi_i - \kappa_i \phi_i) - \left(\frac{\delta g(\phi)}{\delta \phi_i} - \kappa_i \phi_i \right) \tag{2.12}$$

after introducing stabilizer κ_i which satisfies $\kappa_i \geq \frac{1}{2} \max\{0, \max_\phi \frac{\partial^2 g(\phi)}{\partial \phi_i^2}\}$. Correspondingly, the free energy (2.10) can be rewritten as

$$E(\phi) = \int_{\Omega} \left\{ \frac{1}{2} \sum_{i=1}^{M} (\lambda_i |\nabla \phi_i|^2 + \kappa_i \phi_i^2) + \tilde{g}(\phi) \right\} d\mathbf{x}, \tag{2.13}$$

where $\tilde{g}(\phi) = g(\phi) - \frac{1}{2} \sum_{i=1}^{M} \kappa_i \phi_i^2$.

Assuming that function $\tilde{g}(\phi)$ is bounded from below, that is, $\tilde{g}(\phi) \geq -B_0$ for some constant $B_0 \geq 0$. The free energy can be reformed as

$$E(\phi) = \int_{\Omega} \left\{ \frac{1}{2} \sum_{i=1}^{M} (\lambda_i |\nabla \phi_i|^2 + \kappa_i \phi_i^2) + \left(\sqrt{\tilde{g}(\phi) + B_0} \right)^2 - B_0 \right\} d\mathbf{x}. \tag{2.14}$$

Since we only add a zero term $B_0 - B_0$ therein, we emphasize that the free energy is invariant.

By introducing the auxiliary variables $W = \sqrt{\tilde{g}(\phi) + B_0}$ and $\psi_i = \int_\Omega \phi_i d\mathbf{x} - \tilde{N}_i$ $(i = 1, 2, \cdots, M)$, the modified free energy functional can be expressed as the following functional

$$E(\phi, W, \psi) = \int_\Omega \left\{ \frac{1}{2} \sum_{i=1}^M (\lambda_i |\nabla \phi_i|^2 + \kappa_i \phi_i^2) + W^2 - B_0 \right\} d\mathbf{x} + \frac{1}{2} \sum_{i=1}^M P_i \psi_i^2, \quad (2.15)$$

where $\tilde{N}_i = \mathbf{q}_i^T \mathbf{N}$ and P_i are penalty parameters to retain mass constraint for all components.

Based on the variational approach, we have

$$\frac{\partial \phi_i}{\partial t} = -\frac{\delta E(\phi, W, \psi)}{\delta \phi_i} = \lambda_i \Delta \phi_i - \kappa_i \phi_i - W(\phi) H(\phi_i) - P_i \psi_i, \quad (2.16)$$

where $H(\phi_i) = \frac{\frac{\partial \tilde{g}(\phi)}{\partial \phi_i} - \kappa_i \phi_i}{\sqrt{\tilde{g}(\phi) + B_0}}$. Then, we obtain a new, but equivalent partial differential system as follows:

$$\begin{cases} \dfrac{\partial \phi_i}{\partial t} = \lambda_i \Delta \phi_i - \kappa_i \phi_i - W(\phi) H(\phi_i) - P_i \psi_i, & (2.17) \\[2mm] \dfrac{\partial W}{\partial t} = \dfrac{1}{2} \sum_{i=1}^M H(\phi_i) \dfrac{\partial \phi_i}{\partial t}, & (2.18) \\[2mm] \dfrac{\partial \psi_i}{\partial t} = \int_\Omega \dfrac{\partial \phi_i}{\partial t} d\mathbf{x}, & (2.19) \end{cases}$$

with the initial conditions

$$\phi_i|_{(t=0)} = \phi_{i0}, \quad W|_{(t=0)} = \sqrt{\tilde{g}(\phi_{i0}) + B_0}, \quad \psi_i|_{(t=0)} = 0, \quad (2.20)$$

for $i = 1, 2, \cdots, M$.

Denoted by $(h(\mathbf{x}), g(\mathbf{x})) = \int_\Omega h(\mathbf{x}) g(\mathbf{x}) d\mathbf{x}$ the L^2-inner product of two arbitrary functions $h(\mathbf{x})$ and $g(\mathbf{x})$, and $\|g\| = \sqrt{(g,g)}$ the L^2-norm of any function $g(\mathbf{x})$. Taking the L^2-inner product of (2.17) with $\frac{\partial \phi_i}{\partial t}$, of (2.18) with W, and taking the simple multiplication of (2.19) with $P_i \psi_i$, summing them up, we then get the energy dissipation law of the modified system (2.17)-(2.19) as follows

$$\frac{d}{dt} E(\phi, W, \psi) = -\sum_{i=1}^M \left\| \frac{\partial \phi_i}{\partial t} \right\|^2 \leq 0. \quad (2.21)$$

In the following, we focus on designing numerical schemes for time stepping of the transformed system (2.17)-(2.19), that are linear and satisfy discrete energy dissipation laws.

Remark 2.1. For the regularity relation between $\mathbf{n}$ and $\mathbf{\Phi}$, we have the following conclusion from the property of the linear transformation. If $\mathbf{\Phi} \in (H^s(\Omega))^M$ $(s \geq 0)$, then $\mathbf{n} \in (H^s(\Omega))^M$ $(s \geq 0)$, and vice versa.

3   Linear numerical schemes for time integration

In this section we present linear time stepping schemes of first and second order respectively, to solve the system (2.17)-(2.19). Let us assume a uniform time partition with the time step size δt.

3.1   First order scheme

Assuming that ϕ_i^k, W^k and ψ_i^k are already known, then we solve ϕ_i^{k+1}, W^{k+1} and ψ_i^{k+1} from the following first order temporal semi-discretized system: for $i=1,2,\cdots,M$,

$$
\begin{cases}
\dfrac{\phi_i^{k+1}-\phi_i^k}{\delta t}=\lambda_i\Delta\phi_i^{k+1}-\kappa_i\phi_i^{k+1}-W^{k+1}H(\phi_i^k)-P_i\psi_i^{k+1}, & (3.1)\\[3mm]
\dfrac{W^{k+1}-W^k}{\delta t}=\dfrac{1}{2}\sum_{i=1}^{M}H(\phi_i^k)\dfrac{\phi_i^{k+1}-\phi_i^k}{\delta t}, & (3.2)\\[3mm]
\dfrac{\psi_i^{k+1}-\psi_i^k}{\delta t}=\int_\Omega\dfrac{\phi_i^{k+1}-\phi_i^k}{\delta t}d\mathbf{x}. & (3.3)
\end{cases}
$$

From (3.2) and (3.3), we have

$$
W^{k+1}=W^k-\frac{1}{2}\sum_{i=1}^{M}H(\phi_i^k)\phi_i^k+\frac{1}{2}\sum_{i=1}^{M}H(\phi_i^k)\phi_i^{k+1}\triangleq A_{W1}+A_{W2}(\phi_i^{k+1}),
$$

$$
\psi_i^{k+1}=\psi_i^k-\int_\Omega\phi_i^k d\mathbf{x}+\int_\Omega\phi_i^{k+1}d\mathbf{x}\triangleq A_{3i}+A_{4i}(\phi_i^{k+1}).
$$

Then the system (3.1)-(3.3) can be rewritten as

$$
\frac{\phi_i^{k+1}}{\delta t}-\lambda_i\Delta\phi_i^{k+1}+\kappa_i\phi_i^{k+1}+H(\phi_i^k)A_{W2}(\phi_i^{k+1})+P_iA_{4i}(\phi_i^{k+1})
$$
$$
=\frac{\phi_i^k}{\delta t}-H(\phi_i^k)A_{W1}-P_iA_{3i},\quad 1\le i\le M. \tag{3.4}
$$

The above linear system can be denoted as $\mathbb{A}\phi=\mathbf{b}$.

Theorem 3.1. *The linear operator $\mathbb{A}$ is symmetric positive definite.*

Proof. Assuming $\rho=[\rho_1,\rho_2,\cdots,\rho_M]^T$, we have

$$
(\mathbb{A}\phi,\rho)=\frac{1}{\delta t}\sum_{i=1}^{M}(\phi_i,\rho_i)-\sum_{i=1}^{M}\lambda_i(\Delta\phi_i,\rho_i)+\sum_{i=1}^{M}\kappa_i(\phi_i,\rho_i)+\sum_{i=1}^{M}H(\phi_i^k)(A_{W2}(\phi_i),\rho_i)
$$
$$
+\sum_{i=1}^{M}P_i(A_{4i}(\phi_i),\rho_i)
$$

$$= \frac{1}{\delta t} \sum_{i=1}^{M} (\phi_i, \rho_i) - \sum_{i=1}^{M} \lambda_i (\phi_i, \Delta \rho_i) + \sum_{i=1}^{M} \kappa_i (\rho_i, \phi_i) + \sum_{i=1}^{M} H(\phi_i^k)(A_{W2}(\rho_i), \phi_i)$$

$$+ \sum_{i=1}^{M} P_i A_{4i}(\phi_i) A_{4i}(\rho_i)$$

$$= (\mathbb{A}\rho, \phi),$$

and

$$(\mathbb{A}\phi, \phi) = \frac{1}{\delta t} \sum_{i=1}^{M} (\phi_i, \phi_i) - \sum_{i=1}^{M} \lambda_i (\Delta \phi_i, \phi_i) + \sum_{i=1}^{M} \kappa_i (\phi_i, \phi_i) + \sum_{i=1}^{M} H(\phi_i^k)(A_{W2}(\phi_i), \phi_i)$$

$$+ \sum_{i=1}^{M} P_i (A_{4i}(\phi_i), \phi_i)$$

$$= \frac{1}{\delta t} \sum_{i=1}^{M} (\phi_i, \phi_i) + \sum_{i=1}^{M} \lambda_i (\nabla \phi_i, \nabla \phi_i) + \sum_{i=1}^{M} \kappa_i (\phi_i, \phi_i) + \frac{1}{2} \left(\sum_{i=1}^{M} H(\phi_i^k)\phi_i, \sum_{i=1}^{M} H(\phi_i^k)\phi_i \right)$$

$$+ \sum_{i=1}^{M} P_i A_{4i}(\phi_i) A_{4i}(\phi_i)$$

$$\geq \frac{1}{\delta t} \sum_{i=1}^{M} \|\phi_i\|^2.$$

Therefore, the operator $\mathbb{A}$ is symmetric positive definite. $\qquad\square$

Let us define the norm $\|\phi\|_{\mathbb{A}} = \sqrt{(\mathbb{A}\phi, \phi)}$ for any $\phi \in L^2_{per}(\Omega)$ and the subset $\mathbf{X} = \{\phi \in L^2_{per}(\Omega) : \|\phi\|_{\mathbb{A}} < \infty\}$, where $L^2_{per}(\Omega)$ denotes the subspace of all functions $\phi \in L^2(\Omega)$ with periodic or no-flux boundary conditions.

Remark 3.1. It is easy to show that $\|\phi\|_{\mathbb{A}}$ is a norm for $L^2_{per}(\Omega)$ and $\mathbf{X}$ is a Hilbert subspace associated with the norm $\|\phi\|_{\mathbb{A}}$. Then the well-posedness of the linear system $\mathbb{A}\phi = \mathbf{b}$ in the weak sense comes from the Lax-Milgram theorem, i.e., the linear system (3.4) admits a unique weak solution in $\mathbf{X}$.

Theorem 3.2. *The first order linear scheme* (3.1)-(3.3) *is unconditionally energy stable, i.e., satisfies the following discrete energy dissipation law*

$$E_{1st}^{k+1} \leq E_{1st}^{k} - \frac{1}{\delta t} \sum_{i=1}^{M} \|\phi_i^{k+1} - \phi_i^k\|^2, \tag{3.5}$$

where

$$E_{1st}^{k} = \frac{1}{2} \sum_{i=1}^{M} \left(\lambda_i \|\nabla \phi_i^k\|^2 + \kappa_i \|\phi_i^k\|^2 + P_i(\psi_i^k)^2 \right) + \|W^k\|^2. \tag{3.6}$$

Proof. By taking the L^2-inner product of (3.1) with $\phi_i^{k+1}-\phi_i^k$, and summing from $i=1$ to M, we have

$$\frac{1}{\delta t}\sum_{i=1}^{M}\|\phi_i^{k+1}-\phi_i^k\|^2=\sum_{i=1}^{M}\lambda_i\left(\Delta\phi_i^{k+1},\phi_i^{k+1}-\phi_i^k\right)-\sum_{i=1}^{M}\kappa_i\left(\phi_i^{k+1},\phi_i^{k+1}-\phi_i^k\right)$$
$$-\sum_{i=1}^{M}\left(W^{k+1}H(\phi_i^k),\phi_i^{k+1}-\phi_i^k\right)-\sum_{i=1}^{M}P_i\left(\psi_i^{k+1},\phi_i^{k+1}-\phi_i^k\right). \quad (3.7)$$

By taking the L^2-inner product of (3.2) with W^{k+1}, we have

$$2\left(W^{k+1}-W^k,W^{k+1}\right)=\sum_{i=1}^{M}\left(W^{k+1}H(\phi_i^k),\phi_i^{k+1}-\phi_i^k\right). \quad (3.8)$$

By taking the simple multiplication of (3.3) with $P_i\psi_i^{k+1}$, and summing from $i=1$ to M, we obtain

$$\sum_{i=1}^{M}P_i\left(\psi_i^{k+1}-\psi_i^k\right)\psi_i^{k+1}=\sum_{i=1}^{M}P_i\left(\psi_i^{k+1},\phi_i^{k+1}-\phi_i^k\right). \quad (3.9)$$

Combining (3.7)-(3.9), and applying the identity

$$2(a-b,a)=|a|^2-|b|^2+|a-b|^2, \quad (3.10)$$

we obtain

$$\frac{1}{2}\sum_{i=1}^{M}\lambda_i\|\nabla\phi_i^{k+1}\|^2+\|W^{k+1}\|^2+\frac{1}{2}\sum_{i=1}^{M}P_i(\psi_i^{k+1})^2+\frac{1}{2}\sum_{i=1}^{M}\lambda_i\|\nabla\phi_i^{k+1}-\nabla\phi_i^k\|^2+\|W^{k+1}-W^k\|^2$$
$$+\frac{1}{2}\sum_{i=1}^{M}P_i(\psi_i^{k+1}-\psi_i^k)^2+\frac{1}{2}\sum_{i=1}^{M}\kappa\|\phi_i^{k+1}\|^2+\frac{1}{2}\sum_{i=1}^{M}\kappa\|\phi_i^{k+1}-\phi_i^k\|^2$$
$$=\frac{1}{2}\sum_{i=1}^{M}\lambda_i\|\nabla\phi_i^k\|^2+\|W^k\|^2+\frac{1}{2}\sum_{i=1}^{M}P_i(\psi_i^k)^2+\frac{1}{2}\sum_{i=1}^{M}\kappa\|\phi_i^k\|^2-\frac{1}{\delta t}\sum_{i=1}^{M}\|\phi_i^{k+1}-\phi_i^k\|^2. \quad (3.11)$$

Finally, we obtain result (3.5) after dropping some positive terms from Eq. (3.11). □

3.2 Second order scheme

The second order time stepping scheme to solve the system (2.17)-(2.19) is developed based on the second order backward differentiation formulas (BDF2). Assuming that ϕ_i^{k-1}, W^{k-1}, ψ_i^{k-1}, and ϕ_i^k, W^k, ψ_i^k are already known, then we solve ϕ_i^{k+1}, W^{k+1} and ψ_i^{k+1}

from following second order temporal semi-discretized system: for $i=1,2,\cdots,M$,

$$
\begin{cases}
\dfrac{3\phi_i^{k+1}-4\phi_i^k+\phi_i^{k-1}}{2\delta t}=\lambda_i\Delta\phi_i^{k+1}-\kappa_i\phi_i^{k+1}-W^{k+1}H(\phi_i^*)-P_i\psi_i^{k+1}, & (3.12) \\[3mm]
\dfrac{3W^{k+1}-4W^k+W^{k-1}}{2\delta t}=\dfrac{1}{2}\sum_{i=1}^{M}H(\phi_i^*)\dfrac{3\phi_i^{k+1}-4\phi_i^k+\phi_i^{k-1}}{2\delta t}, & (3.13) \\[3mm]
\dfrac{3\psi_i^{k+1}-4\psi_i^k+\psi_i^{k-1}}{2\delta t}=\displaystyle\int_\Omega\dfrac{3\phi_i^{k+1}-4\phi_i^k+\phi_i^{k-1}}{2\delta t}d\mathbf{x}, & (3.14)
\end{cases}
$$

where $\phi_i^*=2\phi_i^k-\phi_i^{k-1}$.

For (3.13) and (3.14), we have

$$
W^{k+1}=\frac{4W^k-W^{k-1}}{3}-\frac{1}{2}\sum_{i=1}^{M}H(\phi_i^*)\frac{4\phi_i^k-\phi_i^{k-1}}{3}+\frac{1}{2}\sum_{i=1}^{M}H(\phi_i^*)\phi_i^{k+1},
$$

$$
\psi_i^{k+1}=\frac{4\psi_i^k-\psi_i^{k-1}}{3}-\int_\Omega\frac{4\phi_i^k-\phi_i^{k-1}}{3}d\mathbf{x}+\int_\Omega\phi_i^{k+1}d\mathbf{x}.
$$

Set

$$
B_1=W^+-\frac{1}{2}\sum_{i=1}^{M}H(\phi_i^*)\phi_i^+,\quad B_2(\phi)=\frac{1}{2}\sum_{i=1}^{M}H(\phi_i^*)\phi_i,
$$

$$
B_{3i}=\psi_i^+-\int_\Omega\phi_i^+d\mathbf{x},\quad B_{4i}(\phi_i)=\int_\Omega\phi_id\mathbf{x},
$$

where $S^+=\frac{4S^k-S^{k-1}}{3}$.

Then, we have the following reduced linear system

$$
\frac{3}{2\delta t}\phi_i^{k+1}-\lambda_i\Delta\phi_i^{k+1}+\kappa_i\phi_i^{k+1}+H(\phi_i^*)B_2(\phi^{k+1})+PB_{4i}(\phi_i^{k+1})
$$

$$
=\frac{1}{2\delta t}(4\phi_i^k-\phi_i^{k-1})-H(\phi_i^*)B_1-PB_{3i},\quad 1\le i\le M. \tag{3.15}
$$

The above linear system can be expressed as $\hat{A}\phi^{k+1}=\hat{\mathbf{b}}$, and we need solve for ϕ^{k+1} from it.

Theorem 3.3. *The linear operator $\hat{A}$ is symmetric positive definite.*

Remark 3.2. Define $\|\phi\|_{\hat{A}}=\sqrt{(\hat{A}\phi,\phi)}$ for any $\phi\in L^2_{per}(\Omega)$ and the subset $\mathbf{X}=\{\phi\in L^2_{per}(\Omega):\|\phi\|_{\hat{A}}<\infty\}$, where $L^2_{per}(\Omega)$ denotes the subspace of all functions $\phi\in L^2(\Omega)$ with periodic or no-flux boundary condition. It is easy to show that $\|\phi\|_{\hat{A}}$ is a norm for $L^2_{per}(\Omega)$ and $\mathbf{X}$ is a Hilbert subspace associated with the norm $\|\phi\|_{\hat{A}}$. Then the well-posedness of the linear system $\hat{A}\phi=\hat{b}$ in the weak sense comes from the Lax-Milgram theorem, i.e., the linear system (3.15) admits a unique weak solution in $\mathbf{X}$.

Theorem 3.4. *The second order linear system* (3.12)-(3.14) *is unconditionally energy stable, that is, satisfies the following discrete energy dissipation law*

$$E_{BDF2}^{k+1,k} \le E_{BDF2}^{k,k-1} - \delta t \sum_{i=1}^{M} \| \frac{3\phi_i^{k+1} - 4\phi_i^k + \phi_i^{k-1}}{2\delta t} \|^2, \tag{3.16}$$

where

$$E_{BDF2}^{k+1,k} = \frac{1}{4} \sum_{i=1}^{M} (\lambda_i (\|\nabla\phi_i^{k+1}\|^2 + \|2\nabla\phi_i^{k+1} - \nabla\phi_i^k\|^2) + \kappa_i (\|\phi_i^{k+1}\|^2 + \|2\phi_i^{k+1} - \phi_i^k\|^2)$$

$$+ P_i((\psi_i^{k+1})^2 + (2\psi_i^{k+1} - \psi_i^k)^2)) + \frac{1}{2}(\|W^{k+1}\|^2 + \|2W^{k+1} - W^k\|^2).$$

4   Numerical experiments

A two-phase (liquid and gas) binary components fluid mixture is simulated to demonstrate the accuracy and efficiency of the first and second order linear schemes in this section. We consider a mixture of two components, namely isobutane (C_4H_{10}) and decane ($C_{10}H_{22}$) in the domain $\Omega = (0, L)^d$ ($d = 2, 3$) with $L = 2.0$E-8 meters. The critical properties and parameters used to compute parameters in Peng-Robinson EOS for each component are listed in Table 1.

Table 1: Critical properties and parameters.

Component	T_c(K)	P_c	ω	m
C_4H_{10}	425.2	3.80 MPa	0.199	0.6708
$C_{10}H_{22}$	617.7	2.10 MPa	0.484	1.0578

The numerical experiments are presented to illustrate the temporal accuracy of our numerical schemes. For initial configuration, we first use the case of one single droplet, that is, the liquid density of the mixture under a saturated pressure condition at the temperature 450K is imposed in a subregion, and the rest of domain is filled with a saturated gas of the mixture under same temperature (Table 2).

Table 2: Initial densities in liquid and gas phases.

Component	Liquid	Gas
C_4H_{10}	4000	500
$C_{10}H_{22}$	3000	500

4.1 Accuracy tests

In order to test the convergence order, starting from a fixed initial configuration obtained by the first order scheme at time $t_0 = 0.5$, we perform our simulations on the time interval $t = [0.5,0.6]$ with refinement time step size $\Delta t = 2.0E-2, 1.0E-2, \cdots, 3.125E-4$ for both the first order (IEQ-1) and the second order (IEQ-BDF2) schemes. We choose the stabilizer coefficients $\kappa_i = 180$, together with a lower bound $1E+12$ and use a 256×256 mesh grid in 2D. We compare each simulated solution with the benchmark obtained by each scheme with $\delta t = 1E-5$. The L^2 relative errors and convergence rates are listed in Table 3.

Table 3: L^2 relative errors and convergence rates in 2D.

Time Step Size Δt	IEQ-1		IEQ-BDF2	
	Error	Conv. rate	Error	Conv. rate
2.0E-2	2.1943E-2	-	1.5156E-2	-
1.0E-2	1.8201E-2	0.27	5.9916E-3	1.34
5.0E-3	1.3570E-2	0.42	1.6472E-3	1.86
2.5E-3	8.9856E-3	0.59	4.4788E-4	1.88
1.25E-3	5.3502E-3	0.75	1.2479E-4	1.84
6.25E-4	2.9414E-3	0.86	3.4321E-5	1.86
3.125E-4	1.5298E-3	0.94	9.1366E-6	1.91

The accuracy in 3D is also tested. The stabilizer coefficient, the low bound and the mesh grid are chosen as $\kappa_i = 180$, $1E+12$ and $128 \times 128 \times 128$, respectively. We compare each simulated solution with the benchmark obtained by each scheme with $\delta t = 1E-5$. The L^2 relative errors and convergence rates are listed in Table 4.

From Table 3 and Table 4, it is easy to observe that both the IEQ-1 and IEQ-BDF2 schemes are very stable for all time step sizes, and have almost first and second order accuracy, respectively. In addition, the second order scheme IEQ-BDF2 gives better accuracy than the first order scheme IEQ-1.

Table 4: L^2 relative errors and convergence rates in 3D.

Time Step Size Δt	IEQ-1		IEQ-BDF2	
	Error	Conv. rate	Error	Conv. rate
2.0E-2	2.1490E-2	-	1.4738E-2	-
1.0E-2	1.7773E-2	0.27	5.7395E-3	1.36
5.0E-3	1.3205E-2	0.43	1.5698E-3	1.87
2.5E-3	8.7156E-3	0.60	4.3159E-4	1.86
1.25E-3	5.1768E-3	0.75	1.2147E-4	1.83
6.25E-4	2.8416E-3	0.87	3.3630E-5	1.85
3.125E-4	1.4766E-3	0.95	9.0771E-6	1.89

4.2   Dynamical evolution in 2D

In this section, we investigate the time evolution of the molar density distribution and the gas-liquid interface in 2D with one droplet and four droplets, respectively. The IEQ-BDF2 scheme with δt=5E-3 is adopted to perform the simulations. The stabilizer coefficients, the lower bound and the mesh grid are chosen as $\kappa_i=180$, 1E+12 and 256×256, respectively.

4.2.1   One droplet

The liquid density of the mixture (single droplet) is filled in the square subdomain of $(\frac{3L}{8},\frac{5L}{8})^2$, and a saturate gas of both components is full of the rest of the domain under the temperature 450K. The simulations of evolution process are shown in Fig. 1 and Fig. 2 at different times ($t=0,0.5,1,2,5,10$) for both components. We can observe that the shape of the droplet for the liquid phase is initially square, then corners are rounded and turning to a circle as system approaching to steady state, and finally the droplet becomes a perfect circle. This coincides with Fig. 3 where the energy decreasing is significant at the beginning and slows down as density of each species is distributed uniformly in all directions and a circular interface is formed, and the mass conservation is well preserved.
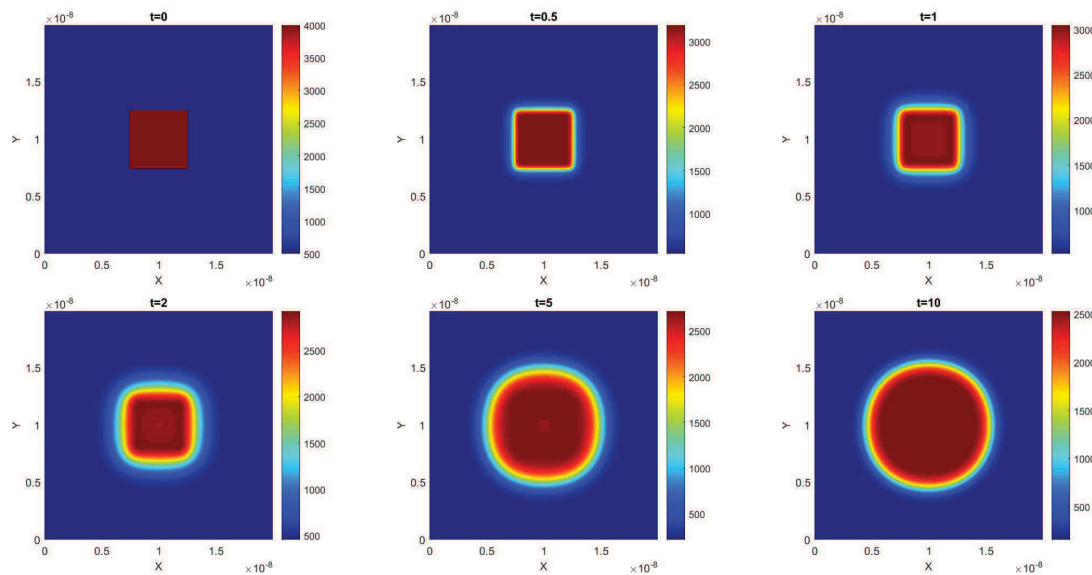
Figure 1: Dynamical evolution of single droplet molar density distribution of C_4H_{10} in 2D. The snapshots are taken at the times $t=0,0.5,1,2,5,10$, respectively.

4.2.2   Four droplets

Next, we simulate the dynamical evolution of molar density distribution for the case of having four droplets as initial configuration, that is, the liquid density of the mixture
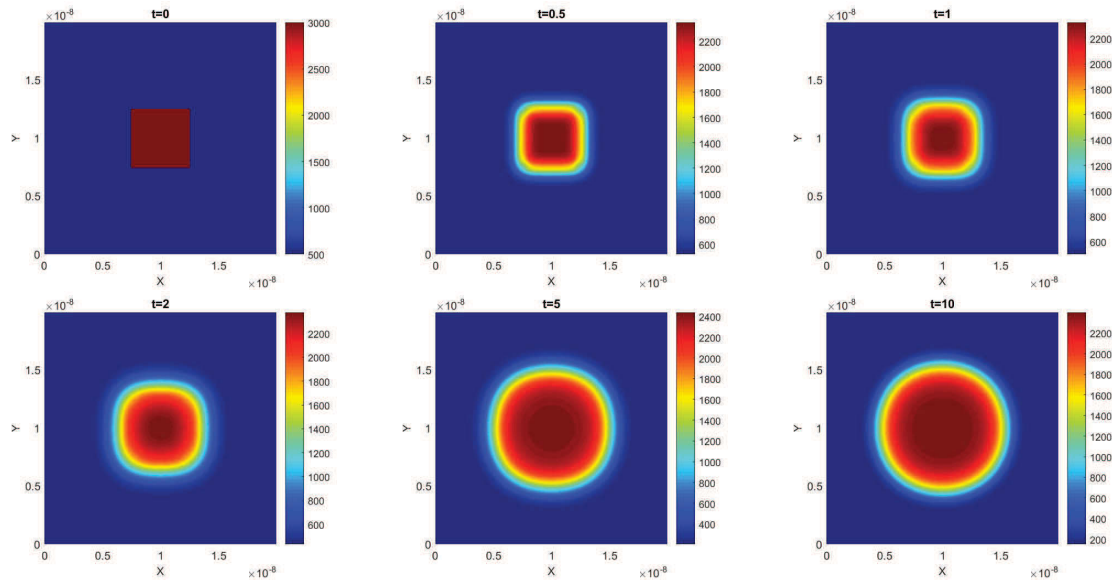
Figure 2: Dynamical evolution of single droplet molar density distribution of $C_{10}H_{22}$ in 2D. The snapshots are taken at the times $t=0,0.5,1,2,5,10$, respectively.
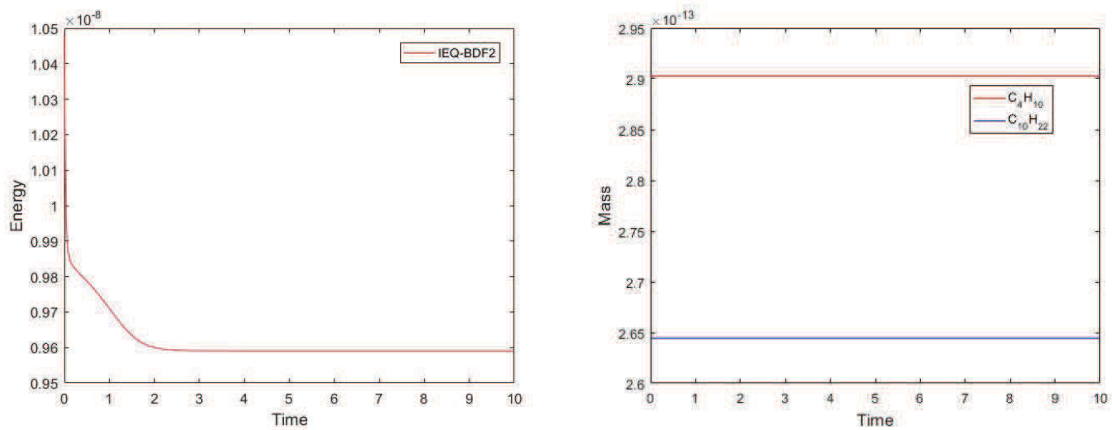

Figure 3: Energy and mass evolutions for the single droplet case simulated by IEQ-BDF2 with $\delta t=$5E-3.

under a saturated pressure condition at the temperature 450K is imposed in the square subregion of $\{(\frac{3L}{16},\frac{7L}{16}),(\frac{9L}{16},\frac{13L}{16})\}^2$, and the rest of domain is filled with a saturated gas of the mixture under same temperature (Table 2). The simulation of evolution process are shown in Fig. 4 and Fig. 5. We observe that the shapes of four droplets are initially square, then four corners are slowly rounded to become circular. Next when the interfaces of droplets start to touch each other, these four droplets start to merge to form one circle-like droplet. In Fig. 6 we plot the evolutions of total energy and mass, and again observe that
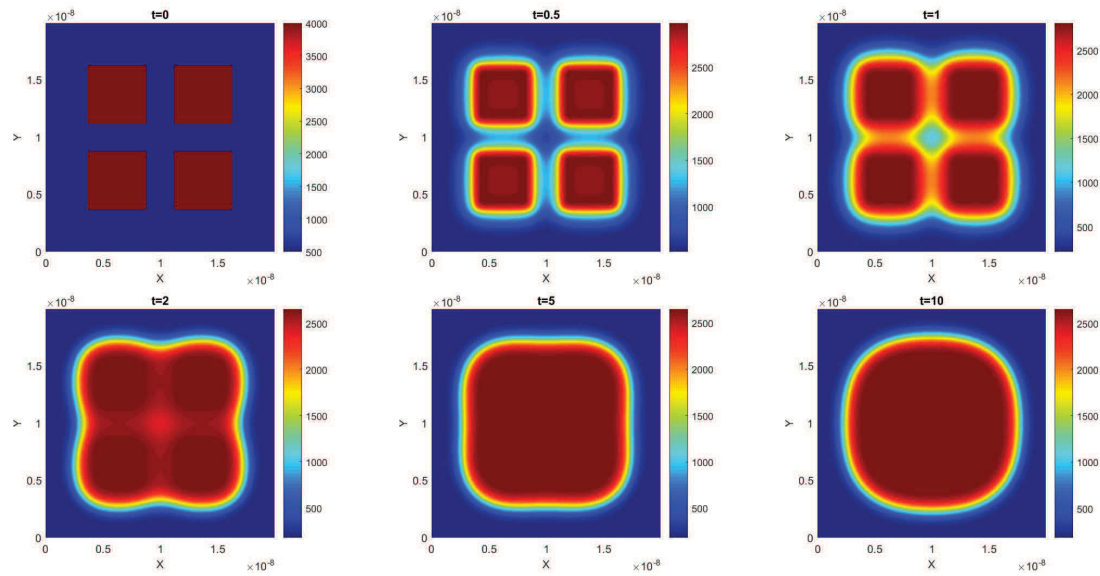
Figure 4: Dynamical evolution of four droplets molar density distribution of C_4H_{10} in 2D. The snapshots are taken at the times $t = 0, 0.5, 1, 2, 5, 10$, respectively.
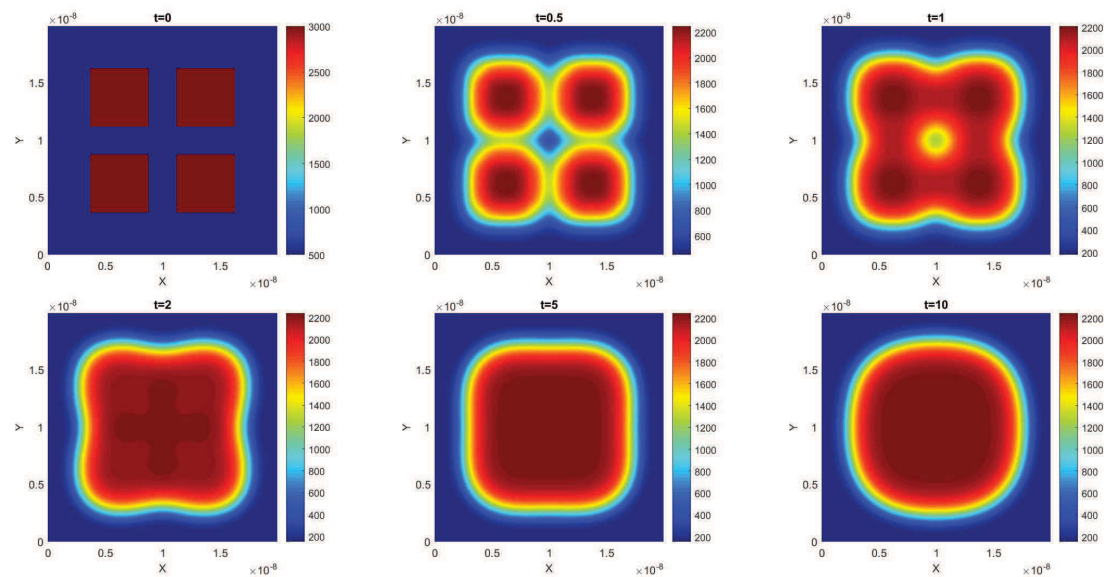

Figure 5: Dynamical evolution of four droplets molar density distribution of $C_{10}H_{22}$ in 2D. The snapshots are taken at the times $t = 0, 0.5, 1, 2, 5, 10$, respectively.

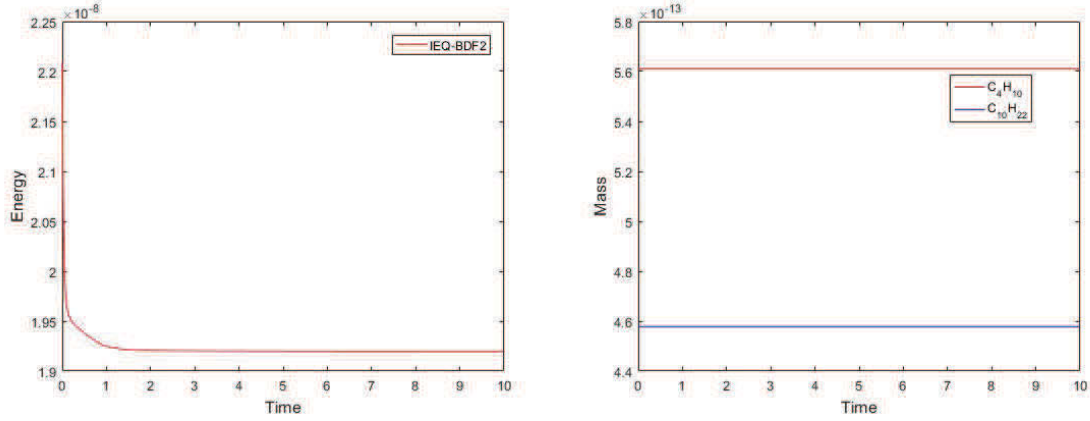the energy decreases monotonically and the mass of each species is accurately maintained along the time.

Figure 6: Energy and mass evolutions for the four droplets case simulated by IEQ-BDF2 with δt=5E-3.

4.3 Dynamical evolution in 3D

Some experiments are presented to simulate the dynamics of the molar density distribution in 3D. We adopt the IEQ-BDF2 scheme with δt=5E-3 and a uniform mesh of $128 \times 128 \times 128$ grid together with a lower bound 1E+12 and the stabilizer coefficients $\kappa_i = 180$.

4.3.1 Single droplet

The first simulation has a single droplet as the initial condition. The liquid density of the mixture under a saturated pressure condition at the temperature 450K is imposed in the cube subregion of $(\frac{3L}{8}, \frac{5L}{8})^3$, and the rest of the cube is filled with a saturated gas of both components under the same temperature.

Fig. 7 and Fig. 8 present the simulated molar density distribution for both components in 3D at different times ($t = 0, 0.5, 1, 2, 5, 10$) during the evolution, respectively. Similar to the dynamical behaviors of a single droplet in 2D, we can observe that the droplet finally forms a sphere and the steady state is reached. The evolutions of the total energy and the mass are plotted in Fig. 9. We can see that the energy decreases monotonically and the masses are accurately maintained along the time. Furthermore, there is a quite large energy decay at the beginning.

4.3.2 Eight droplets

For the initial condition, the liquid density of both components under a saturated pressure condition at the temperature 450K is imposed in the cube subregion of $\left\{ (\frac{3L}{16}, \frac{7L}{16}), (\frac{9L}{16}, \frac{13L}{16}) \right\}^3$, and the rest of the cube is filled with a saturated gas of the mixture under the same temperature.

The simulated molar density distributions for the mixture in 3D at different times ($t = 0, 0.5, 1, 2, 5, 10$) during the evolution are presented in Fig. 10 and Fig. 11. The eight droplets
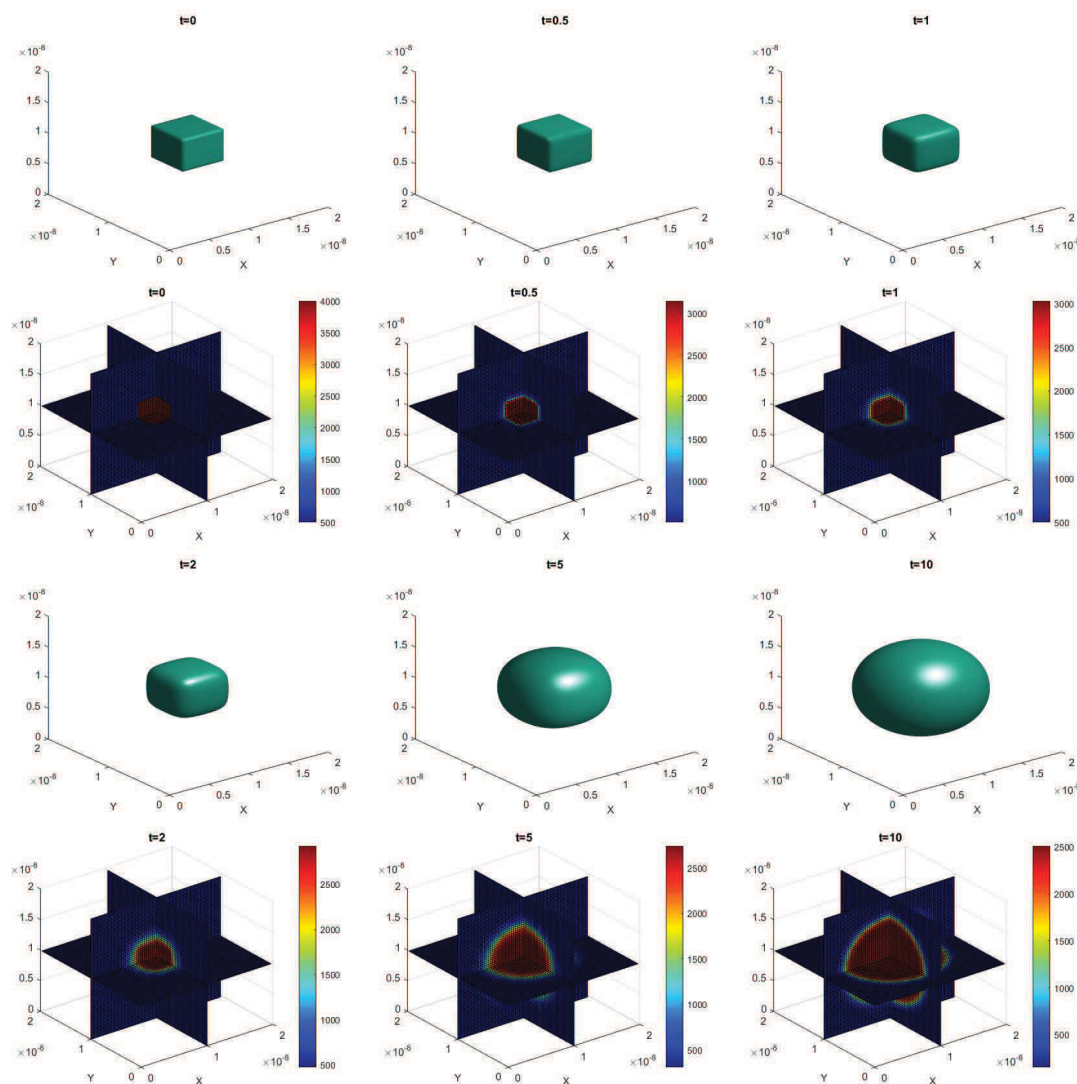
Figure 7: Dynamical evolution of single droplet molar density distribution of C_4H_{10} in 3D. The snapshots are taken at the times $t=0,0.5,1,2,5,10$, respectively. In each time panel, the top one represents the isosurface and the bottom one represents the approximated solution across the three central planes of the 3D cubic domain.

first form to eight separate spheres, then start to merge when their interfaces touch one another and finally become one bigger sphere in the steady state. The dynamical process is very consistent with that of the four droplets case in 2D. We present the evolution of the total energy and the mass with respect to the time in Fig. 12, and observe again the energy monotonically decays and approaches an equilibrium state, and masses are accurately maintained along the time.
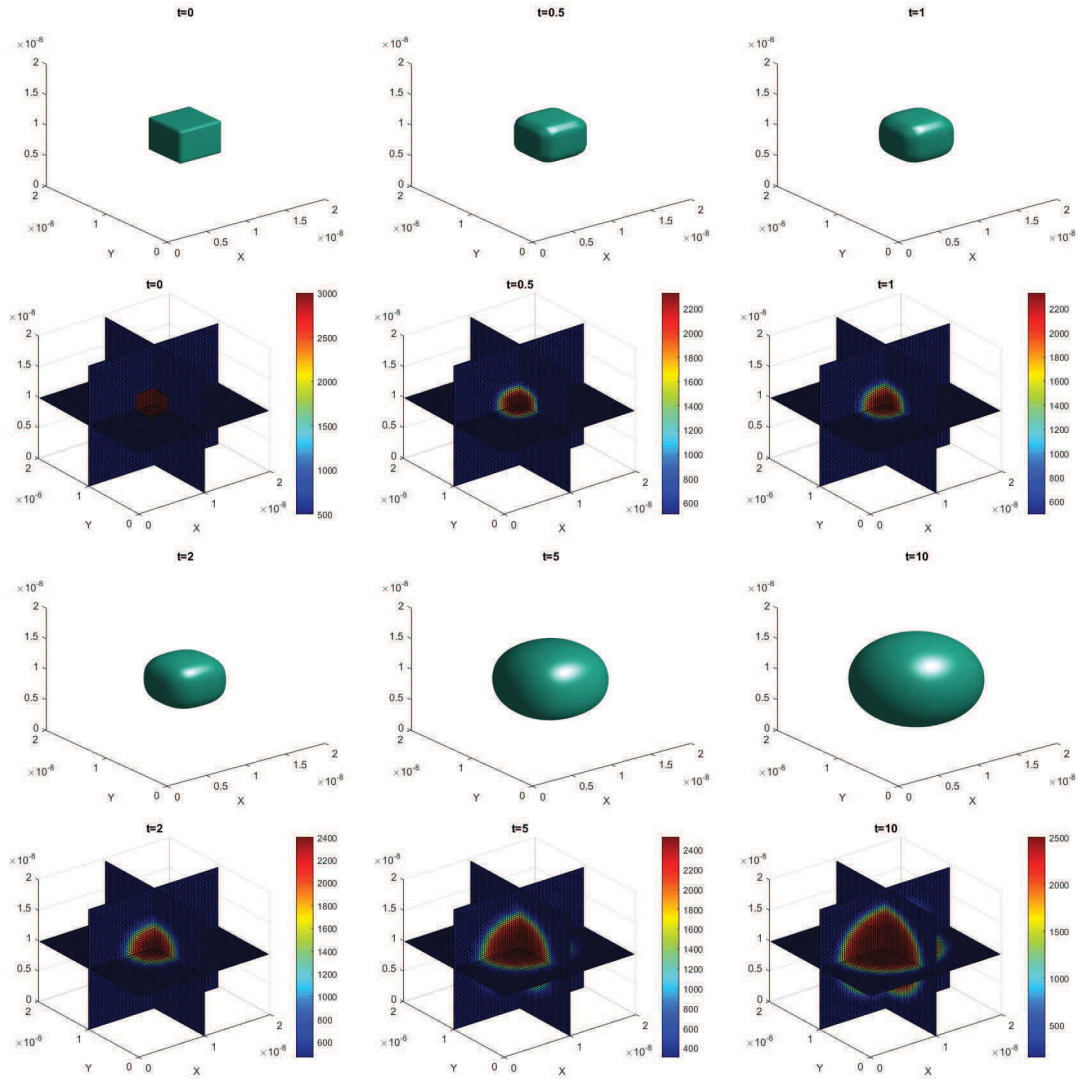
Figure 8: Dynamical evolution of single droplet molar density distribution of $C_{10}H_{22}$ in 3D. The snapshots are taken at the times $t=0,0.5,1,2,5,10$, respectively. In each time panel, the top one represents the isosurface and the bottom one represents the approximated solution across the three central planes of the 3D cubic domain.

5 Conclusions

In this paper, we have designed first and second order linear schemes for time discretization of the multi-component two-phase diffuse interface model with Peng-Robinson equation of state based on the IEQ approach and the stabilized method. The schemes are accurate (up to the second order), unconditionally energy stable, and easy to implement in practice. Moreover, the resulting linear systems in space at each time step are proven
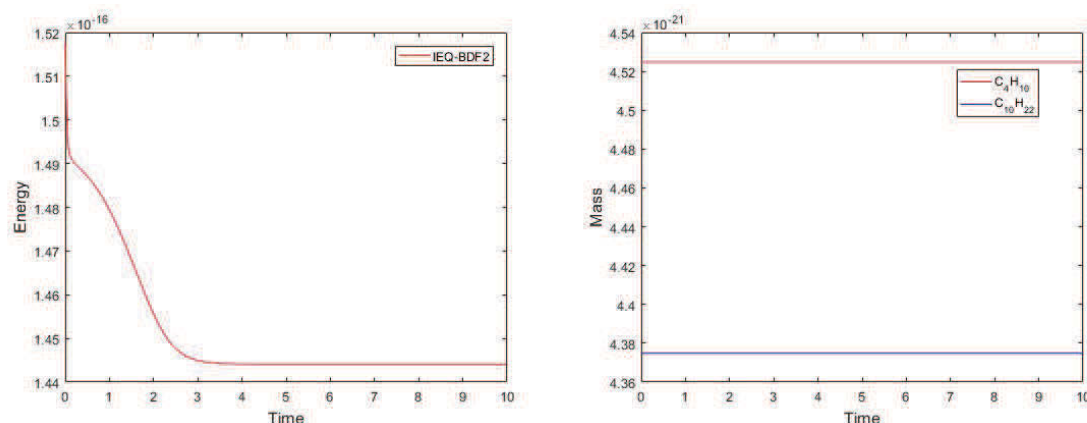
Figure 9: Energy and mass evolutions for the single droplet case simulated by IEQ-BDF2 with δt=5E-3.

to be symmetric positive definite so that one can implement the Krylov subspace methods to solve such system effectively and efficiently. Numerical experiments in two and three dimensional spaces are also presented to demonstrate the accuracy and stability of the schemes, and to illustrate the dynamical evolution of molar density distributions and gas-liquid interfaces.

Acknowledgments

Appendices

A   Parameters

All the following parameters are classical definitions, and can be found in the references [13, 14, 16, 23] and the references cited therein. The universal gas constant R has a value of approximately $8.31432 \mathrm{JK}^{-1}\mathrm{mol}^{-1}$, and the (temperature-dependent) energy parameter $a = a(T)$ and the co-volume parameter b in the Peng-Robinson equation of
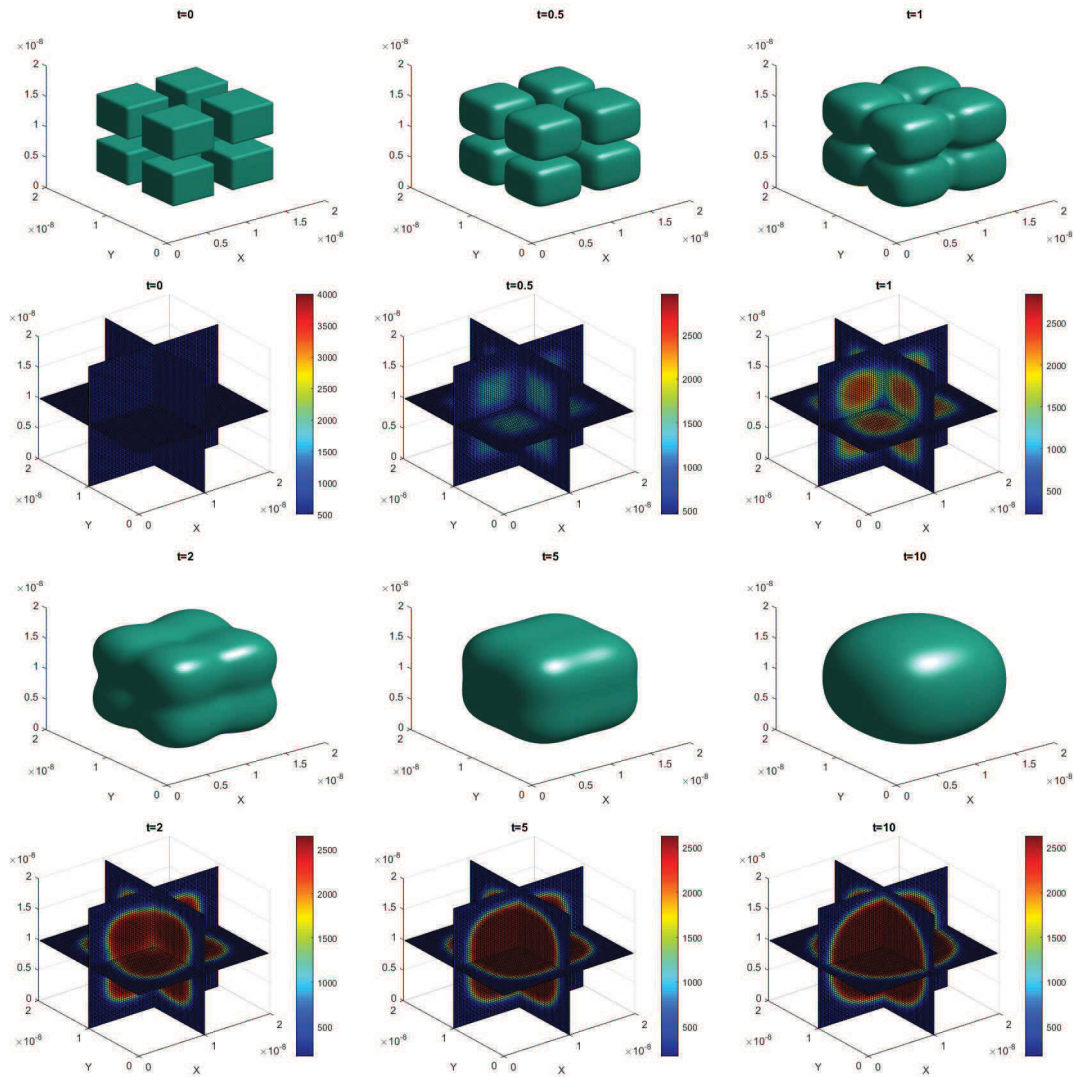
Figure 10: Dynamical evolution of eight droplets molar density distribution of C_4H_{10} in 3D. The snapshots are taken at the times $t=0,0.5,1,2,5,10$, respectively. In each time panel, the top one represents the isosurface and the bottom one represents the approximated solution across the three central planes of the 3D cubic domain.

state are defined as

$$a(T) = \sum_{i=1}^{M} \sum_{j=1}^{M} (1-k_{ij}) y_i y_j \sqrt{a_i(T) a_j(T)}, \qquad b = \sum_{i=1}^{M} y_i b_i,$$

with $y_i = \frac{n_i}{n}$ being the mole fraction of component i. The binary interaction coefficient $0 \le k_{ij} \le 1$ is assumed to be a constant for a fixed species pair and usually computed from experimental correlation. The Peng-Robinson parameters for the pure-substance
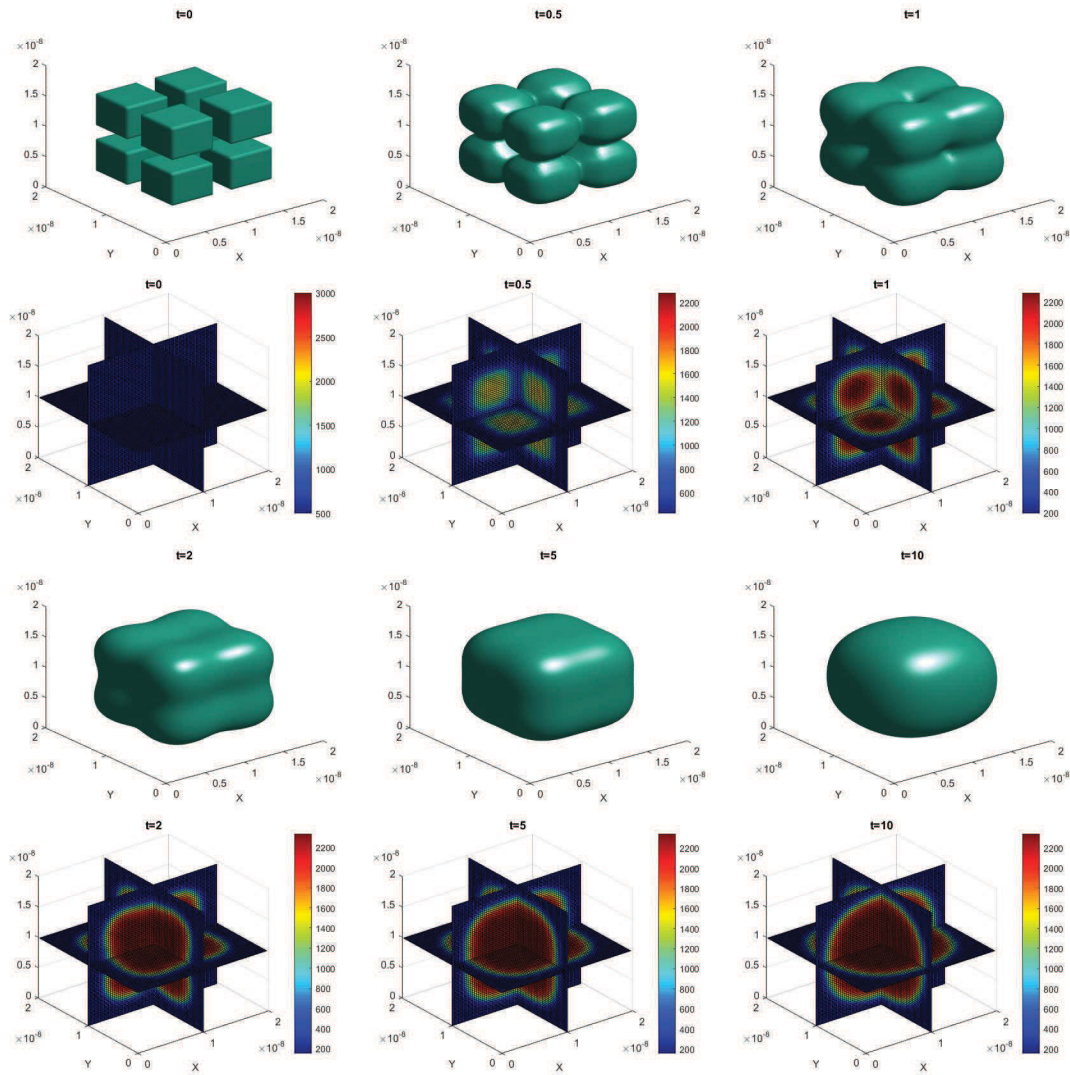
Figure 11: Dynamical evolution of eight droplets molar density distribution of $C_{10}H_{22}$ in 3D. The snapshots are taken at the times $t=0,0.5,1,2,5,10$, respectively. In each time panel, the top one represents the isosurface and the bottom one represents the approximated solution across the three central planes of the 3D cubic domain.

component i, a_i and b_i, are calculated from the critical properties of the specie

$$a_i(T) = 0.45724 \frac{R^2 T_{c_i}^2}{P_{c_i}} \left(1 + m_i \left(1 - \sqrt{\frac{T}{T_{c_i}}}\right)\right)^2,$$
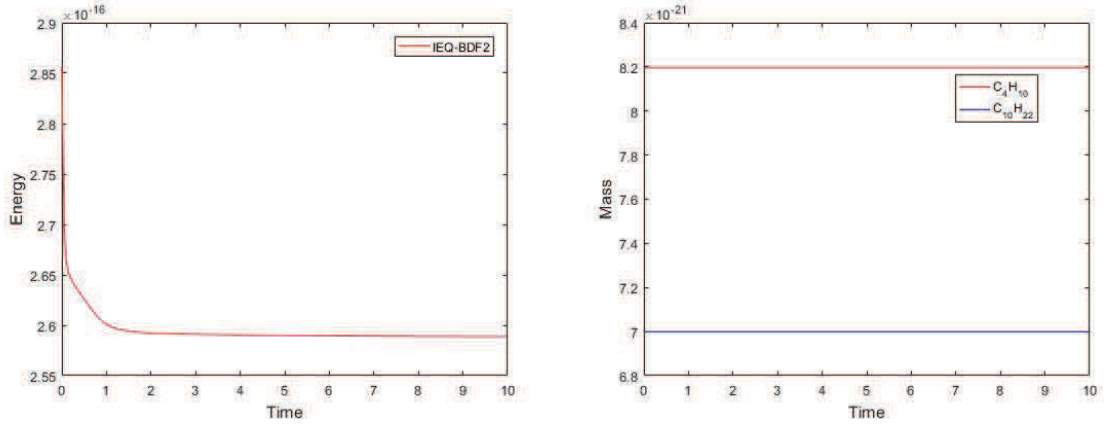
$$b_i = 0.07780 \frac{R T_{c_i}}{P_{c_i}},$$

Figure 12: Energy and mass evolutions for the eight droplets case simulated by IEQ-BDF2 with δt=5E-3.

where T_{c_i} and P_{c_i} represent the critical temperature and pressure of the pure substance component i respectively, which are intrinsic properties of the specie and available for most substances encountered in engineering applications. The parameter m_i for modeling the influence of temperature on a_i is experimentally correlated to the acentric parameter of the specie ω_i by

$$m_i = \begin{cases} 0.37464 \ + 1.54226\omega_i \ -0.26992\omega_i^2, & \omega_i \le 0.49, \\ 0.379642 + 1.485030\omega_i - 0.164423\omega_i^2 + 0.016666\omega_i^3, & \omega_i > 0.49, \end{cases}$$

with

$$\omega_i = \frac{3}{7}\left(\frac{\log_{10}(\frac{P_{c_i}}{14.695\ \text{PSI}})}{\frac{T_{c_i}}{T_{b_i}} - 1} \right) - 1 = \frac{3}{7}\left(\frac{\log_{10}(\frac{P_{c_i}}{1\ \text{atm}})}{\frac{T_{c_i}}{T_{b_i}} - 1} \right) - 1,$$

where T_{b_i} represents the normal boiling point of the pure substance i, "PSI" is "pounds per square inch", and "atm" refers to the standard atmosphere pressure (equal to 101325Pa).

The dependence of the influence parameter c_{ij} on the molar concentrations is in practice very weak, thus it is common to assume that $c_{ij} = c_{ij}(T)$ is just a temperature-dependent parameter, which often can be obtained by adopting the modified geometric mean

$$c_{ij}(T) = (1 - \beta_{ij})\sqrt{c_i(T)c_j(T)}.$$

Note β_{ij} is the binary interaction coefficient for the influence parameter, usually required to be included between 0 and 1 and $\beta_{ij} = \beta_{ji}$ to maintain the stability of the interfaces, and c_i is the influence parameter of the pure substance component i, computed by

$$c_i = a_i b_i^{\frac{2}{3}}\left(m_{1,i}^c\left(1 - \frac{T}{T_{c_i}}\right) + m_{2,i}^c \right)$$

with $m_{1,i}^c$ and $m_{2,i}^c$ being the coefficients correlated merely with the acentric factor ω_i by

$$m_{1,i}^c = -\frac{10^{-16}}{1.2326+1.3757\omega_i}, \qquad m_{2,i}^c = \frac{10^{-16}}{0.9051+1.5410\omega_i}.$$

B   Proof of Theorem 3.3

Proof. Assuming $\rho = [\rho_1, \rho_2, \cdots, \rho_M]^T$, we have

$$\begin{aligned}
(\hat{A}\phi, \rho) &= \frac{3}{2\delta t}\sum_{i=1}^{M}(\phi_i, \rho_i) - \sum_{i=1}^{M}\lambda_i(\Delta\phi_i, \rho_i) + \sum_{i=1}^{M}\kappa_i(\phi_i, \rho_i) + \sum_{i=1}^{M}H(\phi_i^*)(B_2(\phi_i), \rho_i) \\
&\quad + \sum_{i=1}^{M}P_i(B_{4i}(\phi_i), \rho_i) \\
&= \frac{3}{2\delta t}\sum_{i=1}^{M}(\phi_i, \rho_i) - \sum_{i=1}^{M}\lambda_i(\phi_i, \Delta\rho_i) + \sum_{i=1}^{M}\kappa_i(\rho_i, \phi_i) + \sum_{i=1}^{M}H(\phi_i^*)(B_2(\rho_i), \phi_i) \\
&\quad + \sum_{i=1}^{M}P_i B_{4i}(\phi_i) B_{4i}(\rho_i) \\
&= (\hat{A}\rho, \phi),
\end{aligned}$$

and

$$\begin{aligned}
(\hat{A}\phi, \phi) &= \frac{3}{2\delta t}\sum_{i=1}^{M}(\phi_i, \phi_i) - \sum_{i=1}^{M}\lambda_i(\Delta\phi_i, \phi_i) + \sum_{i=1}^{M}\kappa_i(\phi_i, \phi_i) + \sum_{i=1}^{M}H(\phi_i^*)(B_2(\phi_i), \phi_i) \\
&\quad + \sum_{i=1}^{M}P_i(B_{4i}(\phi_i), \phi_i) \\
&= \frac{3}{2\delta t}\sum_{i=1}^{M}(\phi_i, \phi_i) + \sum_{i=1}^{M}\lambda_i(\nabla\phi_i, \nabla\phi_i) + \sum_{i=1}^{M}\kappa_i(\phi_i, \phi_i) + \frac{1}{2}\left(\sum_{i=1}^{M}H(\phi_i^*)\phi_i, \sum_{i=1}^{M}H(\phi_i^*)\phi_i\right) \\
&\quad + \sum_{i=1}^{M}P_i B_{4i}(\phi_i) B_{4i}(\phi_i) \\
&\geq \frac{3}{2\delta t}\sum_{i=1}^{M}\|\phi_i\|^2.
\end{aligned}$$

Therefore, the operator $\hat{A}$ is symmetric positive definite. $\qquad\square$

C   Proof of Theorem 3.4

Proof. By taking the L^2-inner product of (3.12) with $3\phi_i^{k+1} - 4\phi_i^k + \phi_i^{k-1}$, and summing from $i=1$ to M, we have

$$\frac{1}{2\delta t}\sum_{i=1}^{M}\|3\phi_i^{k+1}-4\phi_i^k+\phi_i^{k-1}\|^2$$

$$=\sum_{i=1}^{M}\Big[\lambda_i\Big(\Delta\phi_i^{k+1},3\phi_i^{k+1}-4\phi_i^k+\phi_i^{k-1}\Big)-\kappa_i\Big(\phi_i^{k+1},3\phi_i^{k+1}-4\phi_i^k+\phi_i^{k-1}\Big)$$

$$-\Big(H(\phi_i^*)W^{k+1},3\phi_i^{k+1}-4\phi_i^k+\phi_i^{k-1}\Big)-P_i\Big(\psi_i^{k+1},3\phi_i^{k+1}-4\phi_i^k+\phi_i^{k-1}\Big)\Big]. \qquad \text{(C.1)}$$

By taking the L^2-inner product of (3.13) with W^{k+1}, we obtain

$$(3W^{k+1}-4W^k+W^{k-1},W^{k+1})=\frac{1}{2}\sum_{i=1}^{M}H(\phi_i^*)(3\phi_i^{k+1}-4\phi_i^k+\phi_i^{k-1},W^{k+1}). \qquad \text{(C.2)}$$

By taking the L^2-inner product of (3.14) with $P_i\psi_i^{k+1}$, and summing from $i=1$ to M, we get

$$\sum_{i=1}^{M}P_i(3\psi_i^{k+1}-4\psi_i^k+\psi_i^{k-1})\psi_i^{k+1}=\sum_{i=1}^{M}P_i(\psi_i^{k+1},3\phi_i^{k+1}-4\phi_i^k+\phi_i^{k-1}). \qquad \text{(C.3)}$$

By combining the (C.1)-(C.3), and applying the following identity

$$2(3a-4b+c,a)=|a|^2-|b|^2+|2a-b|^2-|2b-c|^2+|a-2b+c|^2, \qquad \text{(C.4)}$$

we have

$$\frac{1}{2}\sum_{i=1}^{M}\Big[\lambda_i\Big(\|\nabla\phi_i^{k+1}\|^2-\|\nabla\phi_i^k\|^2+\|2\nabla\phi_i^{k+1}-\nabla\phi_i^k\|^2-\|2\nabla\phi_i^k-\nabla\phi_i^{k-1}\|^2$$

$$+\|\nabla\phi_i^{k+1}-2\nabla\phi_i^k+\nabla\phi_i^{k-1}\|^2\Big)+\kappa_i\Big(\|\phi_i^{k+1}\|^2-\|\phi_i^k\|^2+\|2\phi_i^{k+1}-\phi_i^k\|^2$$

$$-\|2\phi_i^k-\phi_i^{k-1}\|^2+\|\phi_i^{k+1}-2\phi_i^k+\phi_i^{k-1}\|^2\Big)+P_i((\psi_i^{k+1})^2-(\psi_i^k)^2+(2\psi_i^{k+1}-\psi_i^k)^2$$

$$-(2\psi_i^k-\psi_i^{k-1})^2+(\psi_i^{k+1}-2\psi_i^k+\psi_i^{k-1})^2)\Big]+\|W^{k+1}\|^2-\|W^k\|^2+\|2W^{k+1}-W^k\|^2$$

$$-\|2W^k-W^{k-1}\|^2+\|W^{k+1}-2W^k+W^{k-1}\|^2$$

$$=-\frac{1}{2\delta t}\sum_{i=1}^{M}\|3\phi_i^{k+1}-4\phi_i^k+\phi_i^{k-1}\|^2. \qquad \text{(C.5)}$$

Dropping some positive terms from (C.5), we finally obtain the result (3.16). $\qquad\square$

References

[1] D.M. Anderson, G.B. McFadden and A. A. Wheeler. Diffuse-interface methods in fluid mechanics. *Ann. Rev. Fluid Mech.*, 30: 139-165, 1998.

[2] V.E. Badalassi, H.D. Ceniceros and S. Banerjee. Computation of multiphase systems with phase field models. *J. Comput. Phys.*, 190: 371-397, 2003.

[3] M. Copetti and C. Elliott. Numerical analysis of the Cahn-Hilliard equation with a logarithmic free energy. *Numer. Math.*, 63: 39-65, 1992.

[4] A. Diegel and S. Walker. A finite element method for a phase field model of nematic liquid crystal droplets. *Commun. Comput. Phys.*, 25: 155-188, 2019.

[5] H. Ding and P.D.M. Spelt. Wetting condition in diffuse interface simulations of contact line motion. *Phys. Rev. E*, 75: 046708, 2007.

[6] C.M. Elliott and A.M. Stuart. The global dynamics of discrete semilinear parabolic equations. *SIAM J. Numer. Anal.*, 30: 1622-1663, 1993.

[7] D.J. Eyre. Unconditionally gradient stable time marching the Cahn-Hilliard equation, in Computational and mathematical models of microstructural evolution (San Francisco, CA, 1998), vol. 529 of Mater. Res. Soc. Sympos. Proc., MRS, Warrendale, PA, 1998, pp. 39-46.

[8] X. Fan, J. Kou, Z. Qiao and S. Sun. A componentwise convex splitting scheme for diffuse interface models with Van der Waals and Peng-Robinson equations of state. *SIAM J. Sci. Comput.*, 39: B1-B28, 2017.

[9] A. Firoozabadi. Thermodynamics of Hydrocarbon Reservoirs, McGraw-Hill, New York, 1999.

[10] J. Glimm, J.W. Grove, X.L. Li, K.M. Shyue, Q. Zhang and Y. Zeng. Three-dimensional front tracking. *SIAM J. Sci. Comput.*, 19: 703-727, 1998.

[11] V.V. Khatavkar, P.D. Anderson, P.C. Duineveld and H.H.E. Meijer. Diffuse interface modeling of droplet impact on a pre-patterned solid surface. *Macromol. Rapid. Commun.*, 26: 298-303, 2005.

[12] J. Kim. Phase-field models for multi-component fluid flows. *Commun. Comput. Phys.*, 12: 613-661, 2012.

[13] J. Kou and S. Sun. An adaptive finite element method for simulating surface tension with the gradient theory of fluid interfaces. *J. Comput. Appl. Math.*, 255: 593-604, 2014.

[14] J. Kou and S. Sun. Numerical methods for a multicomponent two-phase interface model with geometric mean influence parameters. *SIAM J. Sci. Comput.*, 37: B543-B569, 2015.

[15] J. Kou and S. Sun. Unconditionally stable methods for simulating multi-component two-phase interface models with Peng-Robinson equation of state and various boundary conditions. *J. Comput. Appl. Math.*, 291: 158-182, 2016.

[16] J. Kou, S. Sun and X. Wang. Efficient numerical methods for simulating surface tension of multi-component mixtures with the gradient theory of fluid interfaces. *Comput. Methods Appl. Mech. Engrg.*, 292: 92-106, 2015.

[17] J. Kou and S. Sun. Thermodynamically consistent simulation of nonisothermal diffuse-interface two-phase flow with Peng-Robinson equation of state. *J. Comput. Phys.*, 371: 581-605, 2018.

[18] J. Kou and S. Sun. Thermodynamically consistent modeling and simulation of multi-component two-phase flow model with partial miscibility. *Comput. Methods Appl. Mech. Engrg.*, 331: 623-649, 2018.

[19] H. Li, L. Ju, C. Zhang and Q. Peng. Unconditionally energy stable linear schemes for the diffuse interface model with Peng-Robinson equation of state. *J. Sci. Comput.*, 75: 993-1015, 2018.

[20] J.S. Lopez-Echeverry, S. Reif-Acherman and E. Araujo-Lopez. Peng-Robinson equation of state: 40 years through cubics. *Fluid Phase Equilibria*, 447: 39-71, 2017.

[21] L. Ma, R. Chen, X. Yang and H. Zhang. Numerical approximations for Allen-Cahn type

phase field model of two-phase incompressible fluids with moving contact lines. *Commun. Comput. Phys.*, 21: 867-889, 2017.

[22] J. Moortgat, S. Sun and A. Firoozabadi. Compositional modeling of three-phase flow with gravity using higher-order finite element methods. *Water Resour. Res.*, 47: W05511, 2011.

[23] Z. Qiao and S. Sun. Two-phase fluid simulation using a diffuse interface model with Peng-Robinson equation of state. *SIAM J. Sci. Comput.*, 36(4): B708-B728, 2014.

[24] L. Rongy, K.B. Haugen and A. Firoozabadi. Mixing from Fickian diffusion and natural convection in binary non-equilibrium fluid phases. *AIChE J.*, 58: 1336-1345, 2012.

[25] J. Shen, J. Xu and J. Yang. The scalar auxiliary variable (SAV) approach for gradient flows. *J. Comput. Phys.*, 353: 407-416, 2018.

[26] J. Shen, J. Xu and J. Yang. A new class of efficient and robust energy stable schemes for gradient flows. arXiv:1710.01331v1, 2017.

[27] A. Spizzichino, S. Goldring and Y. Feldman. The immersed boundary method: application to two-phase immiscible flows. *Commun. Comput. Phys.*, 25: 107-134, 2019.

[28] S. Sun and M.F. Wheeler. Symmetric and nonsymmetric discontinuous Galerkin methods for reactive transport in porous media. *SIAM J. Numer. Anal.*, 43: 195-219, 2005.

[29] S. Sun and M.F. Wheeler. Local problem-based a posteriori error estimators for discontinuous Galerkin approximations of reactive transport. *Comput. Geosci.*, 11: 87-101, 2007.

[30] X. Wang, L. Ju and Q. Du. Efficient and stable exponential time differencing Runge-Kutta methods for phase field elastic bending energy models. *J. Comput. Phys.*, 316: 21-38, 2016.

[31] C. Wang and S.M. Wise. An energy stable and convergent finite difference scheme for the modified phase field crystal equation. *SIAM J. Numer. Anal.*, 49: 945-969, 2011.

[32] X. Yang. Linear, first and second-order, unconditionally energy stable numerical schemes for the phase field model of homopolymer blends. *J. Comput. Phys.*, 327: 294-316, 2016.

[33] X. Yang. Numerical approximations for the Cahn-Hilliard phase field model of the binary fluid-surfactant system. *J. Sci. Comput.*, 74: 1533-1553, 2018.

[34] X. Yang and D. Han. Linearly first- and second-order, unconditionally energy stable schemes for the phase field crystal equation. *J. Comput. Phys.*, 330: 1116-1134, 2017.

[35] X. Yang and L. Ju. Efficient linear schemes with unconditionally energy stability for the phase field elastic bending energy model. *Comput. Methods Appl. Mech. Engrg.*, 315: 691-712, 2017.

[36] X. Yang and L. Ju. Linear and unconditionally energy stable schemes for the binary fluid surfactant phase field model. *Comput. Methods Appl. Mech. Engrg.*, 318: 1005-1029, 2017.

[37] X. Yang, J. Zhao and Q. Wang. Numerical approximations for the molecular beam epitaxial growth model based on the invariant energy quadratization method. *J. Comput. Phys.*, 333: 104-127, 2017.

[38] J. Zhao, Q. Wang and X. Yang. Numerical approximations for a phase field dendritic crystal growth model based on the invariant energy quadratization approach. *Inter. J. Num. Meth. Engrg.*, 110: 279-300, 2017.

[39] J. Zhu, L. Chen, J. Shen and V. Tikare. Coarsening kinetics from a variable mobility Cahn-Hilliard equation-application of semi-implicit Fourier spectral method. *Phys. Rev. E*, 60: 3564-3572, 1999.

[40] L. Zhu, L. Ju and W. Zhao. Fast high-order compact exponential time differencing Runge-Kutta methods for second-order semilinear parabolic equations. *J. Sci. Comput.*, 67: 1043-1065, 2016.